11-2014

A New Transfer Impedance Based System Equivalent Model for Voltage Stability Analysis

Yang Wang
Wayne State University

Caisheng Wang
Wayne State University

Feng Lin
Wayne State University

Wenyuan Li
Chongqing University

Le Yi Wang
Wayne State University

See next page for additional authors

Publisher Citation

Y. Wang, C. Wang, F. Lin, W. Li, LY Wang, and J. Zhao, "A new transfer impedance based system equivalent model for voltage stability analysis," International Journal of Electrical Power & Energy Systems, Vol. 62, pp. 38–44, Nov. 2014.

Comments

This is the author's accepted version of the article published in International Journal of Electrical Power & Energy Systems. The final publication is found at http://dx.doi.org/10.1016/j.ijepes.2014.04.025

A New Transfer Impedance Based System Equivalent Model For Voltage Stability Analysis

Yang Wang[a], Caisheng Wang[a,*], Feng Lin[a], Wenyuan Li[b,c], Le Yi Wang[a], Junhui Zhao[a]

a: Department of Electrical and Computer Engineering, Wayne State University, Detroit, MI, USA.
wangyanghh@hotmail.com, flin@ece.eng.wayne.edu, lywang@wayne.edu,
Junhui.Zhao@wayne.edu
b: School of Electrical Engineering, Chongqing University, Chongqing, China.
c: BC Hydro and Power Authority, Vancouver, Canada. wen.yuan.li@bchydro.com

Abstract- This paper presents a new transfer impedance based system equivalent model (TISEM) for voltage stability analysis. The TISEM can be used not only to identify the weakest nodes (buses) and system voltage stability, but also to calculate the amount of real and reactive power transferred from the generator nodes to the vulnerable node causing voltage instability. As a result, a full-scale view of voltage stability of the whole system can be presented in front of system operators. This useful information can help operators take proper actions to avoid voltage collapse. The feasibility and effectiveness of the TISEM are further validated in three test systems.

Keywords- Voltage stability, system equivalent, transfer impedance, transfer power

1. Introduction

Due to increasing load demands and various pressing constraints such as economic considerations and environmental regulations, power systems are forced to operate closer to their operating limits and become more prone to voltage instability. In recent years, a considerable number of voltage instability related outage events have occurred around the world and resulted in major system failures such as the U.S.-Canada blackout on August 14, 2003 [1]. Voltage stability has become a major concern in power system planning and operation.

"Voltage stability refers to the ability of a power system to maintain steady voltages at all buses in the system after being subjected to a disturbance from a given initial operating condition."[2] Unlike angle instability, voltage instability often starts in a local network and gradually extends to the whole system. This feature makes the evolution of system losing voltage stability generally slower (in a few seconds or even longer) than that of losing angle stability which could happen quickly in a couple of cycles. Though some voltage instability phenomena can happen really fast, the focus of this paper is given to the long-term voltage stability issues.

It has been observed that voltage magnitude is not a good indication for power system voltage stability estimation [3]. In recent years, therefore, many new voltage stability indices have been proposed in literatures and some of them have been applied in real power systems [4], including the P-V and Q-V curves based methods [5], [6], Jacobian matrix singularity indices [7-9], voltage collapse index based on the distance of power-flow solution pairs [10], L index [11], line-based indices [12-17] and the node-based indices [18-26].

No matter what type of indices is used in voltage stability analysis, one of critical pieces is to obtain an accurate model for the power system under study. A new system equivalent model using the concept of transfer impedance is proposed in this paper, based on which a voltage stability index named equivalent node voltage collapse index (*ENVCI*) is chosen to evaluate system voltage instability. Compared to other system equivalent methods [27]-[28], the proposed method has several unique characteristics: 1) generator internal impedances are included; 2) loads are substituted by corresponding equivalent impedances and included in the system impedance matrix; 3) the impact of generators on the vulnerable nodes can be quantified and ranked by calculating the transfer power. Therefore, the TISEM can be used not only to identify the weakest nodes (buses) causing system voltage instability, but also to evaluate the

impact of generators on the weakest nodes (buses). This feature is especially useful when there are distributed generators deployed in the system [29].

The rest of the paper is organized as follows: Section 2 presents the transfer impedance model, the *ENVCI*, and the approach of transfer power calculation. The feasibility and effectiveness of the proposed model and indices are verified in Section 3 on three test systems, followed by the conclusions drawn in Section 4.

2. Models and Indices

2.1 Transfer Impedance-based System Equivalent Model (TISEM)

As shown in the left part of Fig. 1, a grid can be represented by an active grid with an impedance matrix Z_N and a load impedance Z_k when seen from load node k. Using the superposition theorem, the system state is the combination of two components: the component without considering the load current I_k and the additive component only reflecting the impact of the load current (see the right part in Fig. 1).

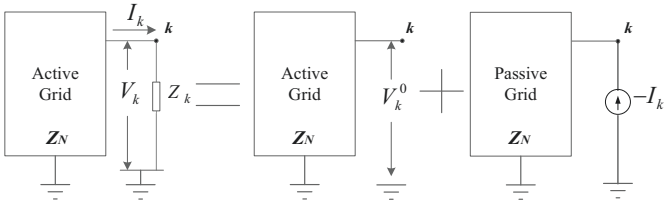

Fig.1. Separation of a grid.

The voltage at node j in the system can be expressed as:

$$V_j = V_j^0 - Z_{jk} I_k \tag{1}$$

where V_j^0 denotes the component of node voltage without Z_k (i.e., bus k is open-circuited); I_k is the load circuit current through Z_k; Z_{jk} is the mutual impedance between nodes j and k. According to the definition of Z_{jk}, the additive voltage component at node j can be calculated as Z_{jk} ($-I_k$). The negative sign here means the negative-current injection at node k. Superscript "0" is used afterwards in the paper to

denote the system states or variables when load Z_k is not added.

The formula given in (1) is general and can also be used for node k:

$$V_k = V_k^0 - Z_{kk} I_k \tag{2}$$

where Z_{kk} is the self-impedance seen from the load node k.

On the other hand, for node k, we have

$$V_k - Z_k I_k = 0 \tag{3}$$

From (2) and (3), the load current can be computed as

$$I_k = \frac{V_k^0}{(Z_{kk} + Z_k)} \tag{4}$$

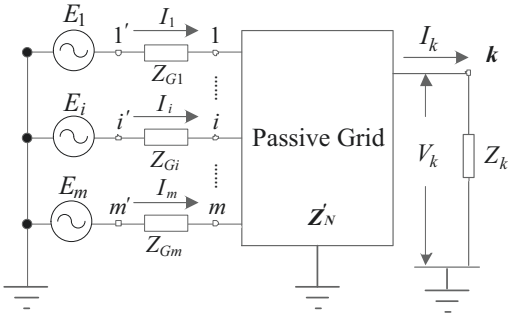

(a) Original network with generators separated

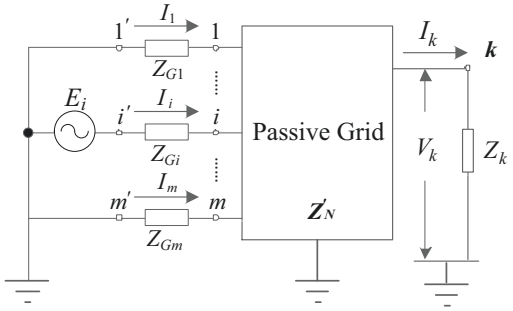

(b) Network with only one generator activated

Fig.2. Application of superposition theorem.

Given m generators in the grid, the grid is re-drawn in Fig. 2(a) by separating all the generators from the active grid.

If only one generator (e.g., the ith generator) is running in the grid and the other generators are removed (see Fig.2 (b)), using (4) and the superposition theorem, the contribution from the ith generator to the total load current (I_k) at bus k can be calculated by

$$I_{k(i)} = \frac{V_{k(i)}^0}{(Z_{kk} + Z_k)} \tag{5}$$

where $I_{k(i)}$ denotes the contribution to the load current from the ith generator; $V_{k(i)}^0$ is the voltage component at the load node k when only the ith generator is active and Z_k is not connected to the system.

Based on the definition of the mutual impedance in impedance matrix $\boldsymbol{Z_N}$, the voltage component at node k when Z_k is not connected is

$$V_{k(i)}^0 = Z_{ik} \frac{E_i}{Z_{Gi}} \tag{6}$$

where E_i and Z_{Gi} are the voltage and the internal impedance of the ith generator; Z_{ik} represents the mutual impedance between nodes i and k. $I_{i(i)}$ represents the current injection at node i when only the ith generator is active.

Substituting (6) into (5) to eliminate $V_{k(i)}^0$ yields

$$I_{k(i)} = \frac{Z_{ik}}{(Z_{kk} + Z_k)} \frac{E_i}{Z_{Gi}} = \frac{E_i}{Z_{Tik}} \tag{7}$$

where $Z_{Tik} = \frac{(Z_{kk} + Z_k)Z_{Gi}}{Z_{ik}}$, which is the transfer impedance between the ith generator (E_i) and bus k with load impedance Z_k included.

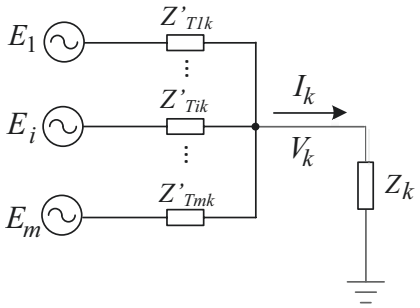

(a) Transfer impedance model

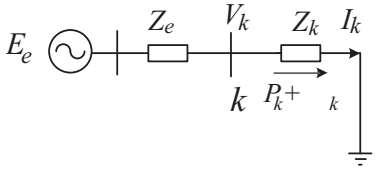

(b) Single-line model

Fig. 3. Transfer impedance-based system equivalent model (TISEM).

The network in Fig. 2 (a) can be converted into an equivalent system using the concept of transfer impedance, as shown in Fig. 3 (a). In the figure, Z'_{Tik} is the transfer impedance between the *i*th generator and bus *k* without including load impedance Z_k. Fig. 3 (a) can be further converted into an overall equivalent circuit of Fig. 3 (b), in which the equivalent impedance Z_{eq} and voltage E_{eq} are $\left(\sum_{i=1}^{m}\frac{1}{Z'_{Tik}}\right)^{-1}$ and $Z_{eq}\left(\sum_{i=1}^{m}\frac{E_i}{Z'_{Tik}}\right)$, respectively. It can be readily proven that Z_{Tik} has a simple relationship with Z'_{Tik} as follows:

$$Z'_{Tik} = \alpha Z_{Tik} \tag{8}$$

where $\alpha = \frac{1}{(1+Z_k/Z_{eq})}$ and

$$Z_{eq} = \left(\sum_{i=1}^{m}\frac{1}{Z_{Tik}}\right)^{-1} - Z_k \tag{9}$$

The derivation process given in (1) – (9) are rigorously based on circuit theories, which guarantees the equivalence of the model given in Fig. 3 at the circuit level. The transfer power (discussed more in the following subsection) from generators to load nodes can be easily calculated from the TISEM, which makes the method unique from other existing ones. It is noted that the transfer impedance (Z_{Tik}) defined in (7) includes load impedance Z_k. Transfer impedance itself is a well established concept and has been commonly used to compute short-circuit currents [30]. Nevertheless, separating load impedance Z_k from the overall transfer impedance to obtain alternative transfer impedance Z'_{Tik} in (8) makes it suitable and useful for voltage stability analysis.

It is worth pointing out that the internal impedance of each generator and the equivalent impedance of each load have already been included in the overall system impedance matrix $\boldsymbol{Z_N}$, except for the load impedance at node *k* which is separately dealt with as the load impedance Z_k that is not included in the system impedance matrix $\boldsymbol{Z_N}$. In other words, impedance matrix $\boldsymbol{Z_N}$ in Fig. 1 and afterwards has

consisted of all line impedances, all generator internal impedances and all instantaneous load impedances except the load impedance at the observed load node k for voltage stability analysis.

It is noted that the load impedance will change with system operating states, for instance, the impedance Z_k at node k can be obtained by

$$Z_k = \frac{V_k}{I_k} = \frac{|V_k|^2}{(P_k + jQ_k)^*} \tag{10}$$

where V_k and I_k are the voltage and current measured at node k; Accordingly, P_k and Q_k are the measured active and reactive power delivered to node k; The superscript "*" denotes the conjugation operation.

TISEM can be readily verified using a simple two-bus system shown in Fig. 4. In the figure, Z_1 represents the generator internal impedance; Z_2 is the impedance of line connecting the nodes 1 and k; Z_3 and Z_k are the equivalent load impedances at nodes 1 and k, respectively, calculated by (10).

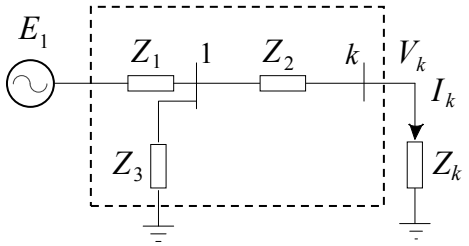

Fig. 4. An example two-bus system.

The admittance matrix Y_N of the system in the dash-line rectangle can be readily established by

$$\boldsymbol{Y_N} = \begin{bmatrix} 1/Z_1 + 1/Z_2 + 1/Z_3 & -1/Z_2 \\ -1/Z_2 & 1/Z_2 \end{bmatrix} \tag{11}$$

The corresponding impedance matrix Z_N without including Z_k is

$$\boldsymbol{Z_N} = \frac{\begin{bmatrix} 1/Z_2 & 1/Z_2 \\ 1/Z_2 & 1/Z_1 + 1/Z_2 + 1/Z_3 \end{bmatrix}}{(1/Z_1 + 1/Z_2 + 1/Z_3)(1/Z_2) - (1/Z_2)^2} \tag{12}$$

The self-impedance at node k is

$$Z_{kk} = \frac{(1/Z_1 + 1/Z_2 + 1/Z_3)}{(1/Z_1 + 1/Z_3)(1/Z_2)} = \frac{1}{1/Z_1 + 1/Z_3} + Z_2 \tag{13}$$

and the mutual impedance between nodes 1and *k* is

$$Z_{1k} = \frac{1/Z_2}{(1/Z_1 + 1/Z_3)(1/Z_2)} = \frac{1}{1/Z_1 + 1/Z_3} \tag{14}$$

According to the equations of $Z_{Tik} = \frac{(Z_{kk} + Z_k)Z_{Gi}}{Z_{ik}}$ and (9), the equivalent transfer impedance regarding node *k* equals to

$$Z_{eq} = (Z_{kk} + Z_k)Z_1 / Z_{1k} - Z_k \tag{15}$$

By substituting Z_{kk} and Z_{1k} into (15), we have

$$Z_{eq} = Z_1 + (Z_2 + Z_k)(Z_1 + Z_3)/Z_3 - Z_k \tag{16}$$

Accordingly, the current through Z_k is calculated as

$$I_k = \frac{E_1}{Z_{eq} + Z_k} = \frac{E_1}{Z_1 + (Z_2 + Z_k)(Z_1 + Z_3)/Z_3} \tag{17}$$

On the other hand, since the components in the two-bus system are connected in simple series and parallel, the load current I_k can be directly observed as

$$\begin{aligned} I_k &= \frac{E_1}{Z_1 + Z_3(Z_2 + Z_k)/(Z_2 + Z_3 + Z_k)} \cdot \frac{Z_3}{Z_2 + Z_3 + Z_k} \\ &= \frac{E_1}{Z_1 + (Z_2 + Z_k)(Z_1 + Z_3)/Z_3} \end{aligned} \tag{18}$$

Obviously, the current calculated by the classic circuit analysis is equal to the value obtained via the TISEM, which verifies the correctness of the method.

2.2 Equivalent node voltage collapse index (*ENVCI*)

For the single-line model in Fig. 3 (b), an equivalent node voltage collapse index (*ENVCI*), which is similar to the one proposed in [25] and [31], can be developed using the TISEM method.

The *ENVCI* can be represented as:

$$ENVCI = 2(e_{eq,x}v_{k,x} + e_{eq,y}v_{k,y}) - (e_{eq,x}^2 + e_{eq,y}^2) \tag{19}$$

In Cartesian coordinate, $E_{eq} = |E_{eq}|\angle\theta_{eq} = e_{eq,x} + je_{eq,y}$, $V_k = |V_k|\angle\theta_k = v_{k,x} + jv_{k,y}$ and $Z_{eq} = R_{eq} + jX_{eq}$.

The expression of *ENVCI* can be also re-written in polar coordinates as

$$ENVCI = 2 \mid E_{eq} \mid\mid V_k \mid \cos\theta - \mid E_{eq} \mid^2 \tag{20}$$

where $\theta = \theta_{eq} - \theta_k$.

Whenever the *ENVCI* of at least one node in the system is zero, it indicates that the system reaches its voltage collapse point. Under an operating condition, obviously, the node with the lowest value of *ENVCI* is the weakest node that may cause system instability for that condition. In other words, the system stability depends on the solvability of the TISEM for all the nodes in a system.

2.3 Transfer power calculation using TISEM

Besides the ability of identifying the weakest nodes and system voltage stability, another unique capability of the TISEM is that it can be used to calculate the transfer power from generator nodes to load nodes. As system voltage instability is closely related to reactive power compensation in a system, the transfer reactive power is used to rank the impacts of generators on the improvement of system voltage stability.

As shown in Fig.3 (a), if node *k* is the weakest node in the system, which is identified by the *ENVCI*, the reactive power transferred from the *i*th generator to node *k* can be calculated by

$$Q_{i,k} = imag\left[V_k \left(\frac{E_i - V_k}{Z'_{Tik}} \right)^* \right] \tag{21}$$

where *imag* is the symbol of taking the imaginary part; Z'_{Tik} represents the transfer impedance without Z_k included and can be calculated by (8).

If several nodes fall into the voltage instability issue simultaneously, the reactive power transferred from the *i*th generator to the vulnerable area is defined as

$$Q_{i,A} = imag\left[\sum_{k\in A} S_{i,k}\right] \tag{22}$$

where A represents the load buses in the weakest area.

Obviously, the generator that provides more reactive power to the weakest node(s) is more important if certain operational actions can be taken at the generator side to improve system voltage stability. In addition to the ability of identifying the weakest nodes using *ENVCI*, a full view of voltage stability of the whole system can be presented in front of system operators. This information is very useful for designing an appropriate reactive power reservation strategy and taking an appropriate control to avoid system voltage collapse.

3. Simulation Results

Simulation studies have been carried out on the IEEE 14-bus system, IEEE 118-bus system and Polish 2746-bus system. The *ENVCI* is calculated for every load nodes in all the three systems. However, due to space limitation, only the *ENVCI* curves regarding the fairly weak nodes are shown in this paper. Moreover, for comparison, the maximum eigenvalues (negative values) and the corresponding bus participation factors (BPF) at the voltage collapse point are calculated using the modal analysis technique [9], as shown in Table 1 below.

Table 1 Maximum Eigenvalue (ME) and Bus Participation Factors (BPF)

Case		Case I	Case II	Case III	Case IV
ME		-0.0437	-0.0688	-0.2999	-0.1790
BPF	2	0.0034	0.0060		
	3	0.0103	0.0247		
	4	0.0194	0.0303		
	5	0.0164	0.0247		
	6	0.0727	0.0859	Bus 74: 0.0464$^{(4)}$	Bus 250: 0.0400$^{(3)}$
	7	0.0587	0.0715	Bus 75: 0.0582$^{(3)}$	Bus 260: 0.0444$^{(2)}$
	8	0.0492	0.0578	Bus 76: 0.6272$^{(1)}$	Bus 450: 0.0377$^{(4)}$
	9	0.0922	0.1045	Bus 118: 0.2594$^{(2)}$	Bus 505: 0.0490$^{(1)}$
	10	0.0932$^{(4)}$	0.1142$^{(3)}$		Bus 2470: 0.0055
	11	0.0850	0.1062		
	12	0.0955$^{(3)}$	0.1096$^{(4)}$		
	13	0.1158$^{(2)}$	0.1168$^{(2)}$		
	14	0.2883$^{(1)}$	0.1478$^{(1)}$		

Note: The weakest nodes (buses) are marked by superscripts (1)-(4) according to their BPF values.

3.1 IEEE14-bus System

The proposed TISEM is first verified using the IEEE14-bus test system as shown in Fig. 5. Two case studies are carried out for the system: Case I for the scenario that the load is increased at one node at a time; and Case II when the loads are increased uniformly at the same time at all the load buses, as suggested by the WECC [32]. In each case, the load power factor is fixed and the amount of load is gradually increased until the IEEE 14-bus system reaches its voltage collapse point. Bus 1 is taken as the slack bus.

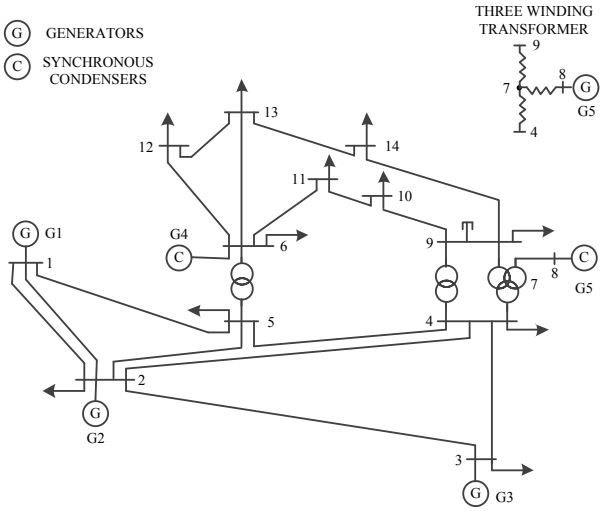

Fig. 5. IEEE14-bus system [33].

3.1.1 Load increase at node 14 (Case I)

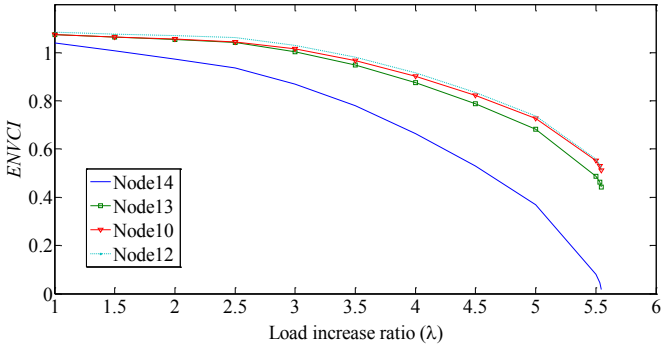

(a) *ENVCI*

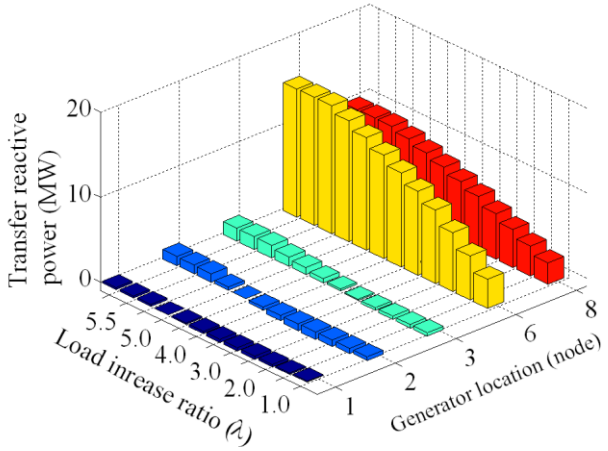

(b) Transfer reactive power to the weakest node

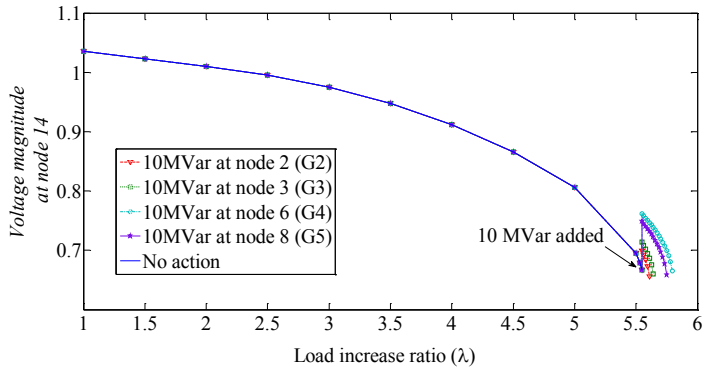

(c) Impact of reactive power compensation at various generator nodes

Fig. 6. Voltage stability profiles as the load increases at node 14 in the IEEE 14 system.

In this case, the load at node 14 is gradually increased while the load power factor is kept as a constant 0.948. The generator at bus 1 takes care of the load increase. As shown in Fig. 6(a), the *ENVCI* points out that the load-increased node (node 14) is the weakest node, followed by nodes 13, 10 and 12. As such, when the system has arrived at its voltage stability limit where the maximum eigenvalue is -0.0437, *ENVCI* at node 14 equals 0.0166, very close to zero, which indicates that the *ENVCI* can effectively identify system voltage stability. Meanwhile, the BPF values in Table 1 judge that the vulnerable nodes follow the order of nodes 14, 13, 12 and 10. There is a small discrepancy in the ordering based on the BPF values and the ordering based on the *ENVCI* values. However, since the BPF values of nodes 10 and 12 (in Table 1) as well as their *ENVCI* values (shown in Fig. 6) are very close, it is still demonstrated that the *EVNCI* can be used to detect the weakest nodes.

In Fig.6 (a), the values of *ENVCI* at nodes 10, 12 and 13 are relatively away from zero, indicating that the voltage stability problems at those nodes have not been serious yet at this load level. Node 14 is the single node causing system voltage collapse under this condition. Therefore, some local enhancement measures such as adding reactive power compensation to node 14 can be used to improve system voltage stability. In the meanwhile, by calculating the transfer power from the generator nodes to the weakest node 14 (shown in Fig.6 (b)), it is observed that the machine at node 6 can affect the weakest node most effectively, followed by node 8, 3, 2 and 1 (slack bus). To further verify the rank, it is assumed that the excitation currents are increased in turn for the generators at nodes 2, 3, 6 and 8 (excluding node 1) to get 10MVar reactive power increase each at a time for those generator nodes. The voltage magnitude changes regarding the various reactive power compensations are plotted in Fig. 6 (c), which shows that the reactive power compensation at node 6 is most effective, followed by nodes 8, 3, 2. This conclusion is completely coincident with the judgment obtained via the transfer power calculations shown in Fig.6 (b).

3.1.2 Load increase at all the load nodes (Case II).

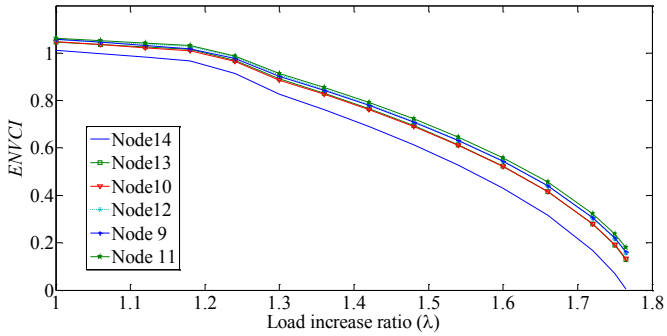

(a) *ENVCI*

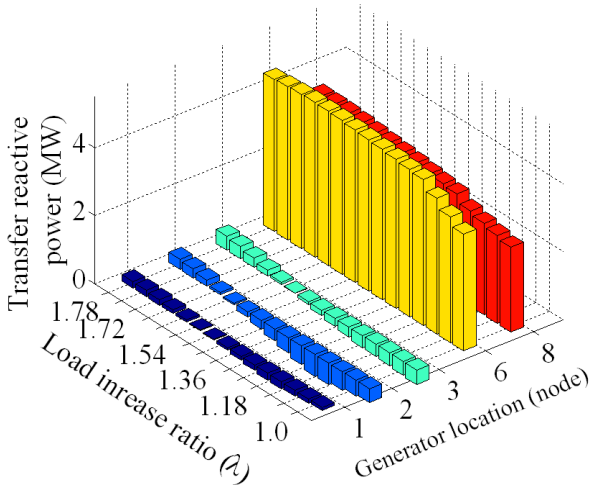

(b) Transfer reactive power to the weakest node

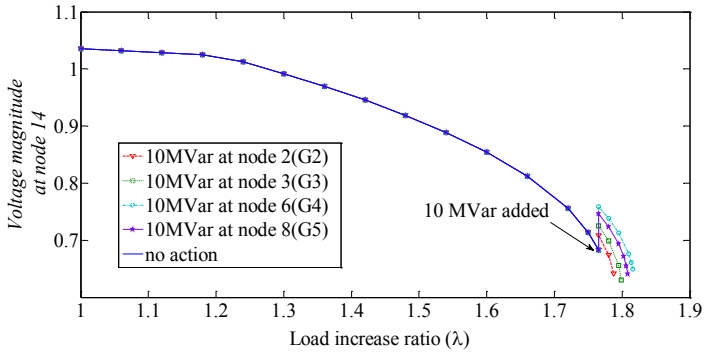

c) Impact of reactive power compensation at various generator nodes

Fig. 7. Voltage stability profiles as the overall load increases in the IEEE 14 system.

As shown in Fig.7 (a), the top four weakest nodes identified by *ENVCI* follow the sequence of nodes 14, 13, 10 and 12, which is consistent with the results of the BPF values in Table 1. Thus, *ENVCI* is also capable of identifying the weakest nodes prone to system voltage instability when the load increases at system wide. Moreover, from Fig. 7(b), based on the amount of reactive power delivered to the weakest node, the generator nodes are ranked as 6, 8, 3, 2, and 1. Such a rank has also been verified by increasing 10MVar reactive power outputs at various generator nodes, as shown in Fig. 7(c).

Fig. 7(a) also shows that node 14 is still the weakest node although the load is increased at all the load nodes. Interestingly, the *ENVCI* values of the majority of load nodes are approaching and close to zero together at the same time. It means that for this case the voltage instability has extended to a relatively wide region. Thus, some full-scale measures, such as increasing the reactive power of

generators, should be taken into priority consideration to improve the voltage stability of the whole system. It is noted that in this case and the cases afterward (i.e., Cases III, and IV) the increased loads are distributed among all the generators in proportion to their power outputs.

3.2 IEEE 118-bus system (Case III)

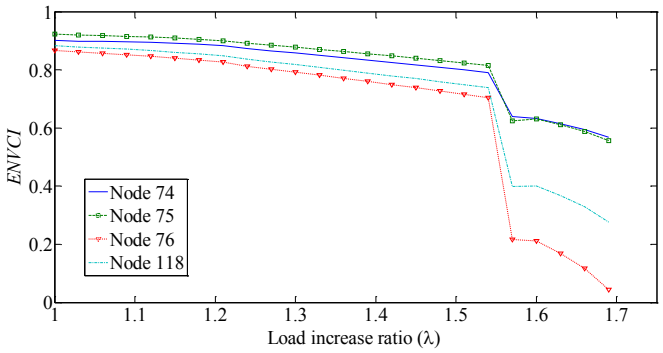

(a) *ENVCI*

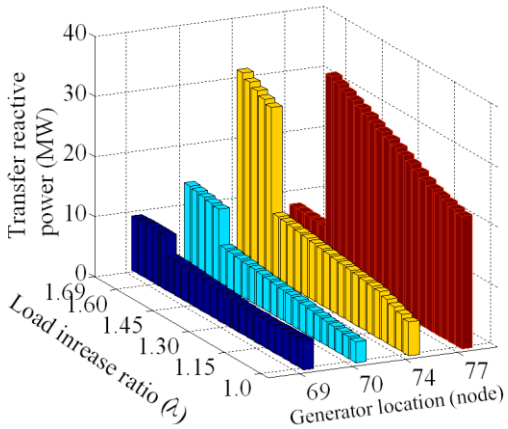

(b) Transfer reactive power to the weakest node.

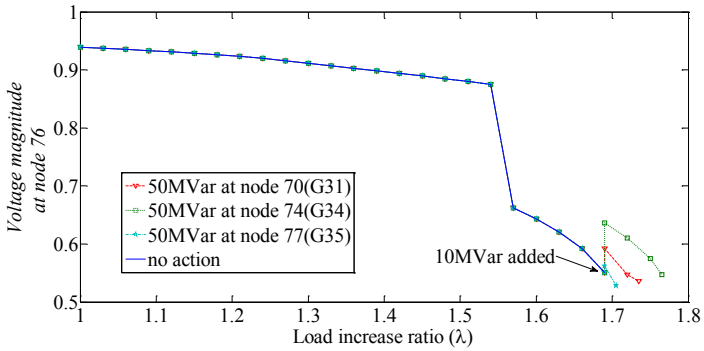

c) Impact of reactive power compensation at various generator nodes

Fig. 8. Voltage stability profiles as the overall load increases in the IEEE 118 system.

In the more complex IEEE 118-bus system [33], the loads at all nodes are increased with the same increase ratio until the system reaches its voltage stability limit. It is assumed that the generator at node 76 is in maintenance and out of service. In the process of load increase, line 76/77 is disconnected from the system due to a grounding fault happened. The *ENVCI*, transfer power to the weakest node, and voltage changes under different reactive power compensations are explored. The simulation results are shown in Figs. 8 (a) – (c), respectively.

In this case, the *ENVCI* has a sharp decrease when line outage happens. The weakest nodes identified by the *ENVCI* are node 76, 118, 75 and 74. In the meanwhile, nodes 76 and 118 are the absolutely key nodes prone to voltage instability. These conclusions can be verified by the *ENVCI* and BPF values, together. Therefore, based on this useful information, planning measures (such as generator installations [29, 34]) or operating measures (such as switching on capacitors [35]) related to these nodes can be applied to improve the voltage stability of the system. According to Fig. 8 (b), if reactive power compensations at the generator side are taken, the top four effective generators are the ones located at nodes 74, 70, 69 and 77, respectively. The voltage changes by increasing the generator reactive power are plotted in Fig. 8 (c). Note that node 69 is operated as a slack bus, so we did not change its reactive power output.

By comparing the TISEM with the eigenvalue method in the simulation studies on the IEEE 14-bus and IEEE 118-bus systems, the following observations can be made:

- Based on the proposed TISEM, the *ENVCI* can identify the weakest node(s) causing voltage instability. Since the range of *ENVCI* is from zero at the voltage collapse point to around 1.0 when the system is pretty secure, it can actually provide a relative margin to estimate how far the current state is apart from the system voltage collapse point.

- By calculating transfer power from generator nodes to load nodes, the most effective generator(s) related to the weakest node(s) in the system can be identified. Therefore, a full-scale view of node voltage stability can be presented in front of system operators. This characteristic of the TISEM can help choose an appropriate control strategy to increase system voltage stability and avoid voltage collapse.

3.3 POLISH 2746-bus system (Case IV)

This case is aimed to further investigate the effectiveness and computational time of the proposed *ENVCI* method in a real POLISH 2746-bus system [36]. The loads at all nodes are also assumed to be increased with the same ratio until the system reaches its voltage stability limit. The weakest node prone to voltage instability is node 2470, followed by nodes 505, 260, 250 and 450, shown in Fig. 9. The result again shows that the *ENVCI* based on TISEM can effectively identify the weakest load node and predict system voltage stability for a real, large power system.

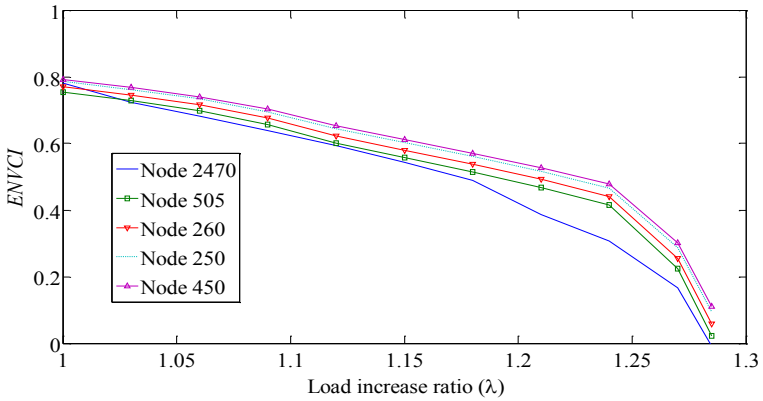

Fig. 9. Voltage stability profiles as the overall load increases in POLISH 2746-bus system.

Table 2 Computational Time

Method \ Case	IEEE 14-bus	IEEE 118-bus	POLISH 2746-bus
TISEM based *ENVCI*	0.0060s	0.0997s	80.8981s
Eigenvalue	0.1690s	2.4367s	2193.7462s

The one-state computational time of the TESEM based *ENVCI* and the eigenvalue method for each of the three test systems is listed in Table 2. All results are obtained using a 5-year old desktop personal

computer with 2.11GHz of CPU and 2.00GB of RAM. Table 3 shows that it takes 80.8981s to calculate the TISEM based *ENVCIs* for the 2746-bus system. It is reasonable to believe that the computational time can be reduced to less than 10s when a more powerful computer is used for the case. This actually can satisfy the requirement in long-term voltage stability analysis in real time as a long-term voltage collapse usually takes longer than 10s to happen [5]. In contrast, the eigenvalue method is about 25 times slower than the TISEM based method. For instance, for the 2746-bus system it needs more than 30mins to get the minimal eigenvalue and relevant bus participation factors. Therefore, the eigenvalue method is not available (N/A) for large systems. Furthermore, it is worth pointing out that for a very large system with tens of thousands of nodes, network reduction techniques [37] can be used to decrease system scale and to increase TISEM calculation speed, but this is out of the scope of this paper.

4. Conclusions

A transfer impedance system equivalent model (TISEM) for system voltage stability evaluation is presented in the paper. Based on the TISEM, the weakest node(s) causing system voltage instability and the most effective generator(s) for improving system voltage stability can be identified, respectively, using the equivalent node voltage collapse index (*ENVCI*) and the amount of transfer power calculated. The proposed model and index have been validated through the theoretical proof and simulation results.

The simulation results of the three test systems have demonstrated the feasibility and effectiveness of the proposed model and index in evaluating the whole system voltage stability, identifying the weakest node(s) in the systems, as well as determining the most effective generator(s). These features can provide useful information not only in monitoring and predicting system voltage instability but also

in taking proper actions to prevent system from voltage collapse for both planning and operation purposes.

References

[1] U.S.-Canada Power System Outage Task Force. Final Report on the August 14, 2003 Blackout in the United States and Canada: Causes and Recommendations. 2004; available at: https://reports.energy.gov/BlackoutFinal-Web.pdf.

[2] IEEE/CIGRE Joint Task Force on Stability Terms and Definitions, Definition and classification of power system stability. IEEE Trans on Power Syst 2004; 19(2): 1387-1401.

[3] Clark, H. K. New challenges: voltage stability. IEEE Power Eng Rev 1990; 10: 33-37.

[4] Glavic, M., and Van Cutsem, T. A short survey of methods for voltage instability detection. IEEE Power and Energy Society General Meeting, Liege, Belgium; July 2011.

[5] Taylor, C. W. Power System Voltage Stability. McGraw-Hill, Inc.; 1994.

[6] Ajjarapu, V. A., and Christy, C. The continuation power flow: A tool for steady-state voltage stability analysis. IEEE Trans on Power Syst 1992; 7 (1): 416-423.

[7] Araposthatis, A., Sastry, S., and Varaiya, P. Analysis of power flow equation. Int J Electr Power Energy Syst 1981; 3(3): 115-126.

[8] Lof, P. A., Smed, T., Anderson, G., and Hill, D. J. Fast calculation of a voltage stability index. IEEE Trans on Power Syst 1992; 7 (1): 54-64.

[9] Gao, B., Morison, G., and Kundur, K. P. Voltage stability evaluation using modal analysis. IEEE Trans on Power Syst 1992; 7(4):. 1529-1542.

[10] Tamura, Y., Mori, H., Lwanoto, S. Relationship between voltage instability and multiple load flow solutions in electrical system. IEEE Trans on Power App and Syst 1983; PAS-102(5): 1115-1125.

[11] Kessel, P., and Glavitsch, H. Estimating the voltage stability of a power system. IEEE Trans on Power Deli 1983; PWRD-1(3): 346-354.

[12] Moghavvemi, M., and Faruque, O. Real-time contingency evaluation and ranking technique. IEEE Proceeding on Gen, Trans and Distr 1998; 145(5): 517-524.

[13] Mohamed, A., Jasmon, G. B., and Yusoff, S. A static voltage collapse indicator using line stability factors. Journal of Industrial Technology 1989; 7(1): 73-85.

[14] Musirin, I., and Rahman, T. K. A. Novel fast voltage stability index (FVSI) for voltage stability analysis in power transmission system. IEEE Proceedings on Student Conference on Research and Development. Shah Alam, Malasia; July 2002.

[15] Venkatesh, B., Ranjan, R., and Gooi, H. B. Optimal reconfiguration of radial distribution systems to maximize loadability. IEEE Trans on Power Syst 2004; 19 (1): 260-266.

[16] Yu, J., Li, W., and Yan, W. A new line loadability index for radial distribution systems. Electric Power Components and Systems 2008; 36 (11): 1245-1252.

[17] Li, W., Yu, J., Wang, Y., Choudhury, P. and Sun, J. Method and system for real time identification of voltage stability via identification of weakest lines and buses contributing to power system collapse. U.S. Patent 7816927, Oct. 2010 (filed Jul. 27, 2007), China Patent Zl200710092710.1, Aug 2009 (filed Sep. 17, 2007).

[18] Vu, K., Begovic, M. M., Novosel, D., and Saha, M. M. Use of local measurements to estimate voltage-stability margin. IEEE Trans on Power Syst 1999; 14(3): 1029-1035.

[19] Arefifar, S. A., and Xu, W. Online tracking of power system impedance parameters and field experiences. IEEE Trans on Power Deli 2009; 24(3): 1781-1788.

[20] Fusco, G., Losi, A., and Russo, M. Constrained least squares methods for parameter tracking of

power system steady-state equivalent circuits. IEEE Trans on Power Deli 2000; 15(3): 1073–1080.

[21] Begovic, M., Milosevic, B., and Novosel, D. A novel method for voltage instability protection. 35th Hawaii International Conference on System Sciences, Hawaii; January 2002.

[22] Eminoglu, U., and Hocaoglu, M. H. A voltage stability index for radial distribution networks. 42nd International Universities Power Engineering Conference, Kocaeli; September 2007.

[23] Brusilowicz, B., Rebizant, W., Szafran, J. Influence of the voltage regulation on the local stability margin of the receiving node. 11th International Conference on Developments in Power Systems Protection, Wroclaw Poland; April 2012.

[24] Corsi, S. Wide area voltage protection. IET Gen, Trans & Distr 2010; 4(10): 1164-1179.

[25] Wang, Y., Li, W., Lu, J. A new node voltage stability index based on local voltage phasors. Elect Power Syst Research 2009; 79(1): 265-271.

[26] Corsi, S. and Taranto, G. N. A real-time voltage instability identification algorithm based on local phasor measurements. IEEE Trans on Power Syst 2008; 23(3): 1271-1279.

[27] Gong, Y., Schulz, N., and Guzman, A. Synchrophasor-based real-time voltage stability index. Proceeding on Power System Conference and Exposition, Atlanta; Oct./Nov. 2006.

[28] Wang, Y. F., Pordanjani, I. R., Li, W., Xu, W., Chen, T., Vaahedi, E., and Gurney, J. Voltage stability monitoring based on the concept of coupled single-port circuit. IEEE Trans on Power Syst 2011; 26 (4): 2154-2163.

[29] Sajjadi, S.M., Haghifam, M.R., Salehi, J., Simultaneous placement of distributed generation and capacitors in distribution networks considering voltage stability index. Int J Electr Power Energy Syst, 46 (2013), pp. 366–375.

[30] Saadat, H. Power System Analysis. McGraw-Hill, Inc; 2004.

[31] Gubina, F. and Strmcnik, B. Voltage collapse proximity index determination using voltage phasor approach. IEEE Trans on Power Syst 1995; 10(2): 788-793.

[32] Abed, A. M. WSCC voltage stability criteria, undervoltage load shedding strategy, and reactive power reserve monitoring methodology. Proceedings on IEEE Power and Energy Society Summer Meeting, San Diego; July 1999.

[33] IEEE test systems, available at: http://www.ee.washington.edu/research/pstca/.

[34] Roselyna, J. P., Devarajb, D., Dasha, S. S., Multi objective differential evolution approach for voltage stability constrained reactive power planning problem, Int J Electr Power Energy Syst, 59 (2014), pp. 155–165.

[35] Balamurugan, G., Aravindhababu, P., Online VAR support estimation for voltage stability enhancement, Int J Electr Power Energy Syst, 49 (2013), pp. 408–413.

[36] Matpower test systems, available at: http://www.pserc.cornell.edu/matpower/.

[37] Yu, J., Li, W., Ajjarapu, V., Yan, W., Zhao, X., Identification and location of long-term voltage instability based on branch equivalent, IET Gen, Trans & Distr 2014; 8(1): 46-54.